MCP-1 Deficiency Delays Regression of Pathologic Retinal Neovascularization in a Model of Ischemic Retinopathy

Michael H. Davies, Andrew J. Stempel, and Michael R. Powers

Purpose. The present study investigates whether retinal neovascularization (NV) and apoptosis are altered in MCP-1–deficient ($^{-/-}$) mice in the OIR model.

Methods. Postnatal day (P) 7 MCP-1$^{-/-}$ and C57BL/6 (B6) mice were exposed to 75% oxygen for 5 days and then recovered in room air. Immunostaining was performed to localize macrophages/microglia within retinal whole mounts and cross-sections. Retinopathy was qualitatively assessed in FITC-dextran–perfused retinas, and preretinal NV was quantified on P17, P21, and P24. TUNEL analysis was used to compare apoptosis between B6 and MCP-1$^{-/-}$ mice.

Results. MCP-1$^{-/-}$ and B6 mice revealed normal vascular development in room air controls and similar vaso-obliteration in oxygen-exposed mice on P12. MCP-1$^{-/-}$ mice exhibited significantly reduced vascular tuft–associated F4/80^{+} cells compared with B6 mice. FITC-dextran–perfused retinas exhibited prominent neovascular tufts on P17, and quantification of preretinal nuclei revealed no significant differences between MCP-1$^{-/-}$ and B6 mice. In contrast, on P21 and P24, MCP-1$^{-/-}$ mice exhibited significant increases in preretinal neovascular nuclei compared with B6 controls. These increases in NV in the MCP-1$^{-/-}$ mice were associated with a significant reduction in vascular tuft apoptosis.

Conclusions. The results demonstrate that the absence of MCP-1 does not alter normal retinal vascular development. Furthermore, MCP-1$^{-/-}$ mice exhibit a similar neovascular response on P17. However, the reduction in tuft-associated macrophages/microglia in the MCP-1$^{-/-}$ mice correlates with reduced vascular tuft apoptosis and delayed regression of retinal NV. These findings suggest that macrophages/microglia may contribute to tuft regression through their proapoptotic properties. (*Invest Ophthalmol Vis Sci.* 2008;49:4195–4202) DOI:10.1167/iovs.07-1491

Pathologic angiogenesis is a key component of many diverse diseases, including ischemic retinopathies.[1,2] A balance between proangiogenic and antiangiogenic factors determines whether endothelial cells (ECs) will proliferate, migrate, and incorporate into pathologic vessels or undergo apoptosis, causing the nascent vessels to regress.[3] Our laboratory and others[4–6] have reported that Fas-ligand (FasL) can play a counterbalancing role to the proangiogenic growth factors in the eye. Pigment epithelial-derived factor (PEDF) and thrombospondin-1, potent endogenous inhibitors of angiogenesis, induce EC apoptosis through the Fas/FasL pathway.[7] Activated macrophages can induce apoptosis in target cells, including ECs, through cell surface FasL, tumor necrosis factor-alpha (TNF-α), and TNF-related apoptosis-inducing ligand (TRAIL).[8–13]

Activated resident and infiltrating macrophages are dynamic cell populations that have the potential to play multiple roles in disease pathogenesis and development.[14] In addition to their proapoptotic properties during postnatal disease, macrophages are required for EC apoptosis during the regression of ocular capillaries in normal eye development, as demonstrated in the seminal studies by Lang et al.[15,16] In contrast, macrophages are a rich source of angiogenic cytokines and have been linked to choroidal, tumoral, and inflammatory angiogenesis.[17–20] These studies suggest that macrophages/microglia have the potential to play dual roles during pathologic angiogenesis.

Several laboratories have reported the immunolocalization of microglia and macrophages to preretinal neovascular tufts in the mouse model of oxygen-induced retinopathy (OIR).[21–24] As shown in our previous study, the F4/80^{+} population peaks on postnatal day (P) 17 to P21 in the OIR model, which is associated with a significant increase in the chemokine monocyte chemoattractant protein-1 (MCP-1, CCL2) on P17. Proliferation of resident microglia was not observed, suggesting the increase in F4/80^{+} cells is secondary to infiltrating monocytes/macrophages.[22] To further characterize the role that macrophages/microglia play in retinal neovascularization (NV), vascular tuft regression, or both, we used MCP-1–deficient mice (MCP-1$^{-/-}$) in the OIR model. The mouse OIR model reproducibly develops preretinal NV but is also characterized by the predictable regression of neovascular tufts through apoptosis.[5,24,25] In several models of inflammation and injury, MCP-1$^{-/-}$ mice consistently exhibit a reduction in infiltrating macrophages, with an associated alteration in tissue injury.[26–30] Therefore, using MCP-1$^{-/-}$ mice in the model of OIR should help clarify the role of infiltrating macrophages in this model of retinal NV.

Materials and Methods

Animals

Breeding pairs of C57BL/6 (B6) mice and MCP-1$^{-/-}$ mice (on a B6 background) were purchased from The Jackson Laboratory (Bar Harbor, ME), provided food and water ad libitum, and kept on a 12-hour light/12-hour dark cycle. Mice were housed and bred in the Oregon Health & Science University animal care facilities and were treated in compliance with the National Institutes of Health guidelines and the guidelines outlined in the ARVO Statement for the Use of Animals in Ophthalmic and Vision Research. Using the mouse model of OIR established by Smith et al,[25] MCP-1$^{-/-}$ and B6 control pups, along with nursing females, were exposed to 75% oxygen for 5 days beginning on

From the Departments of Pediatrics and Ophthalmology, Casey Eye Institute, Oregon Health & Science University, Portland, Oregon.

Supported by National Eye Institute Grants EY011548 (MRP) and EY10572 (core grant); the Medical Research Foundation of Oregon (MRP); and Research to Prevent Blindness.

Submitted for publication November 20, 2007; revised April 25, 2008; accepted July 17, 2008.

Disclosure: **M.H. Davies**, None; **A.J. Stempel**, None; **M.R. Powers**, None

The publication costs of this article were defrayed in part by page charge payment. This article must therefore be marked "*advertisement*" in accordance with 18 U.S.C. §1734 solely to indicate this fact.

Corresponding author: Michael R. Powers, Departments of Pediatrics and Ophthalmology, Casey Eye Institute, Oregon Health & Science University, Mail Code L467IM, 3181 SW Sam Jackson Park Road, Portland, OR 97239-4197; powersm@ohsu.edu.

Copyright © Association for Research in Vision and Ophthalmology

Downloaded from iovs.arvojournals.org on 04/13/2021

P7 and then allowed to recover in room air on P12. Room air control litters of MCP-$1^{-/-}$ and B6 mice were maintained in conditions identical to those for the hyperoxia-exposed animals. Hyperoxia-exposed (O_2 [O_2 refers to hyperoxia exposed between P7 and P12]) and room air control pups were killed by CO_2 euthanatization or cervical dislocation on P12, P14, P17, P21, and P24. One eye was carefully enucleated from each mouse and was placed in 10% neutral-buffered formalin overnight and routinely processed for paraffin embedding. These eyes were sectioned at 5-μm intervals, mounted on slides (SuperFrost Plus; Fisher Scientific, Pittsburgh, PA), and stored at room temperature until used for immunohistologic and TUNEL analysis. The retina of the contralateral eye was dissected for mRNA isolation and analysis, and subsets of mice were used for retinal flat mount studies.

Immunohistochemistry

To assess microglia and macrophages, retinal whole mounts and cross-sections were immunolabeled as previously described.[22] Briefly, for whole mount analysis, the eyes were enucleated, and the lenses and retina were dissected out and fixed in 4% paraformaldehyde (PFA). The lenses were removed, and the retinas were incubated with a rat anti–mouse F4/80 antigen antibody (Serotec, Raleigh, NC) for 36 to 48 hours at 4°C. Retinas were incubated with biotinylated rabbit anti–rat IgG (Vector Laboratories, Burlingame, CA). ABC-AP complex (Vector) was applied to retinas and visualized (Fast Red; BioGenex Laboratories, San Ramon, CA). Retinas were incised radially, and the vitreous was removed and flat mounted with antifade (SlowFade; Molecular Probes, Eugene, OR).

Retinal tissue sections were routinely deparaffinized and rehydrated before antigen retrieval by proteolytic digestion with 0.1% trypsin (Sigma, St. Louis, MO) for 5 minutes at room temperature. After a 1-hour blocking step in 2% goat serum, sections were incubated overnight at 4°C with F4/80 antibody in a humidifying chamber. Sections were incubated with an FITC-conjugated goat anti-rat IgG antibody (Serotec), counterstained with DAPI, and mounted with antifade (SlowFade; Molecular Probes).

Retinal whole mounts and cross-sections were visualized by light and fluorescence microscopy and were photographed with a digital camera (DC500; Leica Microsystems, Bensheim, Germany). To quantitate the F4/80$^+$-labeled cells of B6 and MCP-$1^{-/-}$ mice, vascular tufts from P17O_2 retinas were photographed in a masked fashion (2–4 images/section) using four representative sections 60 μm apart ($n = 8$ eyes). F4/80$^+$ cells were then counted in a masked fashion from the digital images (B6, $n = 53$; MCP-$1^{-/-}$, $n = 53$). Additional tissue sections were used for evaluation of intraretinal blood vessels after immunolocalization with a type IV collagen antibody (Collaborative Biomedical Products, Bedford, MA), as previously described.[5]

Retinal Fluorescein Angiography

Qualitative assessment of retinal vasculature was performed on hyperoxia-exposed and room air control mice at P12, P17, and P21.[31] Mice were given a general anesthetic cocktail, injected subcutaneously, that contained ketamine, xylazine, and acepromazine. Mice were then perfused through the left ventricle with a solution of 1 mL PBS and 50 mg high molecular–weight (2×10^6), FITC-conjugated dextran (Sigma). Animals were killed by cervical dislocation, eyes were enucleated, and lenses and retinas were dissected away and fixed in 4% PFA for 3 hours at 4°C. The lens was removed, and the retina was incised radially. After the vitreous was removed, the retina was flat mounted with antifade (SlowFade; Molecular Probes). Retinal vessels were visualized by fluorescence microscopy and photographed with a digital camera (DC500; Leica).

Neovascular Nuclei Quantification

NV was quantified by counting the vascular nuclei that extended anterior to the internal limiting membrane in hematoxylin and eosin–stained sections. Retinal vascular nuclei were counted in a masked fashion and averaged, avoiding hyaloid vessel nuclei near the optic disc and lens (P17O_2 and P21O_2, $n = 1$ eye each from 8 to 10 animals, 15 sections per eye; P24O_2, $n = 1$ eye each from 4 animals, 15 sections per eye). Data are expressed as mean ± SEM.

Apoptosis Analysis

TUNEL assay was performed on retinal cross-sections from hyperoxia-exposed MCP-$1^{-/-}$ and B6 mice, comparing the degree of apoptosis occurring in the neovascular tufts on both P17O_2 ($n = 8$ eyes, 10 sections per eye) and P21O_2 ($n = 6$ eyes, 10 sections per eye). Sections were labeled with the use of a detection kit (Apoptag Peroxidase In Situ Apoptosis Detection Kit; Intergen, Purchase, NY) according to the manufacturer's instructions. After labeling the exposed 3′-OH ends of DNA fragments, apoptotic cells were visualized with DAB substrate and counterstained with methyl green. While taking care to avoid the optic nerve, representative sections were assessed for TUNEL$^+$ cells located beyond the inner-limiting membrane and were quantified in a masked fashion. Data are expressed as mean ± SEM.

To further characterize the apoptotic response, a subset of sections was immunolabeled with an activated caspase-3 antibody. Briefly, after deparaffinization and rehydration, sections were boiled in 1 mM EDTA for antigen retrieval. After a blocking step, sections were incubated overnight at 4°C with cleaved caspase-3 antibody (Cell Signaling, Danvers, MA). Retinal sections were then incubated with biotinylated goat anti–rabbit IgG (Vector). ABC-HRP complex (Vector) was applied, visualized with DAB substrate, and counterstained with methyl green.

Quantitative RT-PCR

Retinas were dissected on P14, P17, and P21 from room air and hyperoxia-exposed B6 mice and pooled ($n = 4$) for RNA analysis. For comparison on the peak day of NV, P17 hyperoxia-exposed MCP-$1^{-/-}$ retinas were also dissected and pooled for RNA analysis. RNA was extracted using Qiagen columns (RNeasy; Qiagen, Valencia, CA) according to manufacturer's instructions. Total RNA was purified by DNase treatment to remove potential genomic DNA contamination. cDNA was then synthesized using oligo(dT)-primed M-MLV reverse transcriptase (Promega, Madison, WI) for 2 hours at 37°C. Relative mRNA expression of F4/80 normalized to β-actin was quantified in triplicate by real-time PCR using a thermocycler (Chromo4; MJ Research, Watertown, MA) and supermix (iQ SYBR Green; Bio-Rad, Hercules, CA). Annealing temperatures and plate-read temperatures were predetermined using control mRNA. Melting curves were determined after product formation, and samples were run on a gel to confirm product size. A standard curve was generated and amplified simultaneously, allowing for determination of relative concentrations of unknown samples. Concentrations are reported in relative fluorescent units. Mouse-specific primer sets were synthesized by Integrated DNA Technologies, Inc. (Coralville, IA) for the following F4/80 sequences: sense, 5′-CGCTGCTGGTTGAATACAGAGA-3′; antisense, 5′-CGGTTGAGCAGACAGTGAATGA-3′. A primer pair for the constitutively expressed β-actin gene was included in each assay as an internal loading control, as follows: sense, 5′-ATGCCAACACAGTGCTGTCT-3′; antisense, 5′-AAGCACTTGCGGTGCACGAT-3′.

Statistical Analysis

Results are expressed as the mean ± SEM. Statistical significance was determined using the Student's *t*-test for comparison between 2 groups or one-way ANOVA for multiple-group comparison (Prism; GraphPad, San Diego, CA). $P < 0.05$ was considered statistically significant in all statistical analyses used.

Results

Reduced Retinal F4/80$^+$ Cells in MCP-1–Deficient Mice

We examined retinal flat mounts and cross-sections using the macrophage/microglia marker F4/80 to determine whether

Downloaded from iovs.arvojournals.org on 04/13/2021

MCP-1$^{-/-}$ mice exhibited reduced macrophage infiltration. Whole mount immunostaining for F4/80 antigen in B6 room air control mice demonstrated F4/80^{+} cells throughout the retina on P17 (Figs. 1A, 1D). In comparison, the P17O$_2$ B6 retinas showed a marked increase in F4/80^{+} cells throughout the retina (Figs. 1B, 1E). However, the increase in F4/80^{+} cells was substantially reduced in the P17O$_2$ MCP-1$^{-/-}$ mice, as observed in the retinal flat mounts (Figs. 1C, 1F). This observation was confirmed by evaluating retinal cross-sections with immunohistochemistry. As previously described, the F4/80 antibody labels microglia in the inner plexiform layer and the outer plexiform layer in B6 room air control retinas on P17 (Fig. 1G, arrows).[21] In contrast to the room air controls, B6 mice exhibited numerous F4/80^{+} cells surrounding the neovascular tufts on P17 in the oxygen-injured retinas, as reported previously (Fig. 1H, arrow).[22] An increase in mRNA expression of retinal F4/80 correlated with increased F4/80^{+} cells observed in B6 oxygen-exposed retinas compared with room air controls (Fig. 1J). The F4/80 PCR results correlate with our previous quantification of retinal F4/80^{+} cells in the OIR model.[22] Similar to the flat mount results, the retinal cross-sections showed that the MCP-1$^{-/-}$ mice exhibited reduced numbers of F4/80^{+} cells in the retina (Fig. 1I, arrow). F4/80^{+} cells were also quantified in retinal cross-sections, and there was a significant reduction in the MCP-1$^{-/-}$ mice compared with B6 mice on P17O$_2$ (Fig. 1K). Real-time PCR also revealed a reduction in F4/80 expression in MCP-1$^{-/-}$ mice compared with B6 controls on P17O$_2$ (Fig. 1L). Despite the reduction in F4/80^{+} cells, the microglia still appeared to have migrated from the plexiform layers to the anterior retina in the hyperoxia-exposed MCP-1$^{-/-}$ mice, similar to the B6 mice (Figs. 1H, 1I).

Delayed Regression of Neovascular Tufts in MCP-1–Deficient Mice

Fluorescein-perfused retinal flat mounts and type IV collagen–immunostained retinal sections revealed similar retinal vascular development on P12 in room air control B6 and MCP-1$^{-/-}$ mice (data not shown). Hyperoxia-exposed B6 and MCP-1$^{-/-}$ mice exhibited central vaso-obliteration (asterisks) and a delay in development of the deep vascular network on P12O$_2$, as previously described (Figs. 2A, 2B).[5] In addition, the superficial and deep networks exhibited a similar degree of vaso-obliteration in type IV collagen–immunostained retinal sections in B6 and MCP-1$^{-/-}$ mice on P12O$_2$ (data not shown). Fluorescein angiography also revealed a similar pattern of avascular regions (asterisks) on P17O$_2$ in B6 and MCP-1$^{-/-}$ mice (Figs. 2C, 2D). Higher magnification of retinal flat mounts on P17O$_2$ demonstrated a similar neovascular response in B6 and MCP-1$^{-/-}$ mice (Figs. 2E, 2F). On P21O$_2$, B6 mice experienced vascular tortuosity but decreased NV, as shown in fluorescein-perfused flat mounts (Fig. 2G), whereas MCP-1$^{-/-}$ mice continued to exhibit numerous neovascular tufts (Figs. 2H, arrows).

The extent of retinal NV was quantified in cross-sections by counting the average number of vascular nuclei extending beyond the inner limiting membrane (Fig. 3). On P17O$_2$, the peak day of NV, hyperoxia-exposed B6 and MCP-1$^{-/-}$ mice exhibited similar degrees of preretinal NV (arrows), with 24.7 ± 5.3 and 24.6 ± 1.3 preretinal nuclei per cross-section, respectively (Figs. 3A, 3B). By P21O$_2$, the average number of preretinal nuclei per section had decreased substantially in the hyperoxia-exposed B6 mice to 6.7 ± 1.1 (Fig. 3C). Such vascular regression is typical for this model.[24,25] In contrast, MCP-

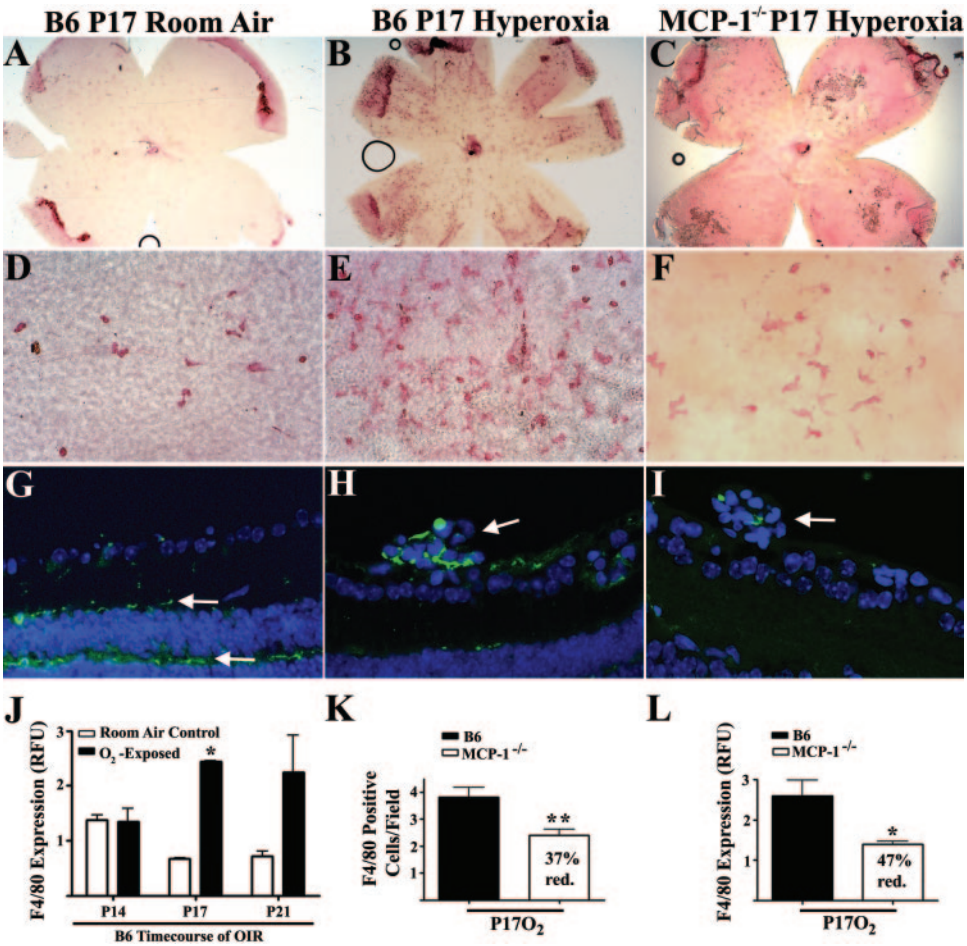

FIGURE 1. Reduced F4/80^{+} macrophages/microglia in MCP-1$^{-/-}$ mice. F4/80-labeled cells (*red*) were localized in retinal whole mounts from B6 room air control mice (**A**, **D**), along with B6 hyperoxia-exposed mice (**B**, **E**), and from MCP-1$^{-/-}$ mice (**C**, **F**). Compared with P17 room air control B6 mice (**A**, **D**), an increase in F4/80-positive cells was observed in hyperoxia-exposed B6 mice (**B**, **E**). Examination of the hyperoxia-exposed MCP-1$^{-/-}$ mice (**C**, **F**) demonstrated a reduced number of F4/80^{+} cells compared with hyperoxia-exposed B6 mice (**B**, **E**) on P17. Immunolabeling of F4/80^{+} macrophages/microglia (*green*) in retinal cross-sections revealed cells localized in the inner plexiform layer on P17 in B6 room air controls (**G**, *arrows*). However, in P17 hyperoxia-exposed retinal cross-sections, F4/80^{+} cells were located within the neovascular tufts in the B6 mice (**H**, *arrow*), whereas fewer macrophages/microglia were associated with tufts in the MCP-1$^{-/-}$ mice (**I**, *arrow*). Original magnifications: (**A–C**) ×25; (**D–I**) ×400. Quantitative real-time PCR for F4/80 expression normalized to β-actin in B6 OIR time course (**J**) and in MCP-1$^{-/-}$ mice compared with B6 mice on P17O$_2$ (**L**). Quantification of F4/80^{+} cells (**K**) in retinal cross-sections. $^{**}P < 0.002$; $^{*}P < 0.05$.

Downloaded from iovs.arvojournals.org on 04/13/2021

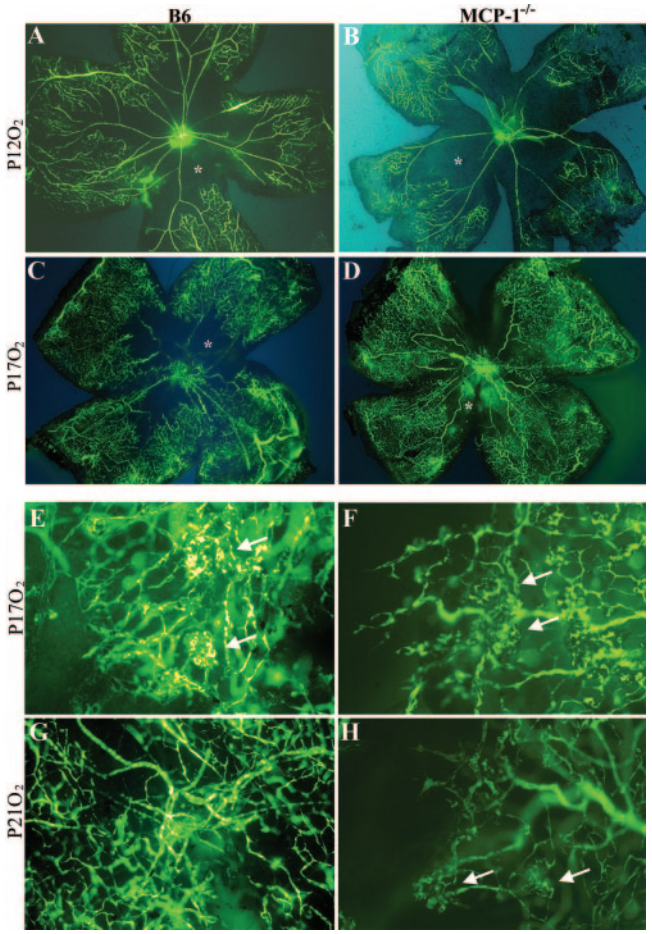

FIGURE 2. Flat-mounted retinas from B6 and MCP-$1^{-/-}$ mice perfused with FITC-dextran. Central retinal vaso-obliteration (*asterisks*) was observed in hyperoxia-exposed B6 (**A**) mice and in hyperoxia-exposed MCP-$1^{-/-}$ (**B**) mice on P12. Retinal neovascularization was evident on P17 in B6 (**C**) and MCP-$1^{-/-}$ (**D**) hyperoxia-exposed mice after 5 days of room air recovery. Avascular regions (*asterisks*) remained present on P17 in both strains of mice. Higher magnification on P17 revealed that, similar to the B6 control mice (**E**), MCP-$1^{-/-}$ retinas (**F**) exhibited a robust neovascular response and had numerous neovascular tufts (*arrows*). By P21, the neovascular response was attenuated in the B6 mice (**G**). In contrast, on P21 the MCP-$1^{-/-}$ hyperoxia-exposed mice exhibited a prolonged neovascular response (**H**), with several residual tufts remaining (*arrows*). Original magnifications: (**A–D**) ×25; (**E–H**) ×400.

$1^{-/-}$ mice continued to have a significant number of preretinal neovascular nuclei, 30.1 ± 6.1, on $P21O_2$ (Fig. 3D). Despite continued vascular regression in hyperoxia-exposed B6 and MCP-$1^{-/-}$ mice on $P24O_2$, a difference persisted in the number of preretinal vascular tuft nuclei per cross-section (1.3 ± 0.28 vs. 9.9 ± 2.2, respectively; Figs. 3E, 3F). The numeric differences in preretinal neovascular nuclei are also depicted in graphical form (Fig. 3G). These observations indicate that the absence of the macrophage chemokine MCP-1 was not associated with reduced retinal NV on $P17O_2$ but rather with delayed regression of retinal NV on $P21O_2$ and $P24O_2$ in the MCP $^{-/-}$ mice compared with the B6 mice.

Reduced Vascular Tuft Apoptosis in MCP-1–Deficient Mice

To determine whether the absence of MCP-1 alters the retina's apoptotic response during vascular tuft regression, TUNEL staining was performed to label apoptotic cells. The apoptotic cells located exclusively within the neovascular tufts were quantified and normalized as a percentage of neovascular nuclei. Compared with the relatively high percentage of $TUNEL^+$ cells (arrows) seen in the hyperoxia-exposed P17 B6 mice (9.9% ± 1.1%; Fig. 4A), a significant decrease in preretinal apoptotic cells (arrows) was observed in hyperoxia-exposed MCP-$1^{-/-}$ mice on P17 (1.6% ± 0.5%; Fig. 4B). Percentage differences for $P17O_2$ preretinal $TUNEL^+$ cells are represented in graphical form (Fig. 4E). The reduction of tuft apoptosis on $P17O_2$ in the MCP-$1^{-/-}$ mice correlated with the reduced number of infiltrating macrophages observed in the MCP-$1^{-/-}$ mice. In contrast to $P17O_2$, the percentage of $TUNEL^+$ cells was not significantly different on $P21O_2$ between the B6 (Fig. 4C) and the MCP-$1^{-/-}$ (Fig. 4D) mice (15.1% ± 4.3% and 8.6% ± 2.8%, respectively; Fig. 4E). However, the relative increase in tuft apoptosis on $P21O_2$ compared with $P17O_2$ (8.6% ± 2.8% vs. 1.6% ± 0.5%) in the MCP-$1^{-/-}$ mice correlated with the gradual regression of the NV observed between $P21O_2$ and $P24O_2$.

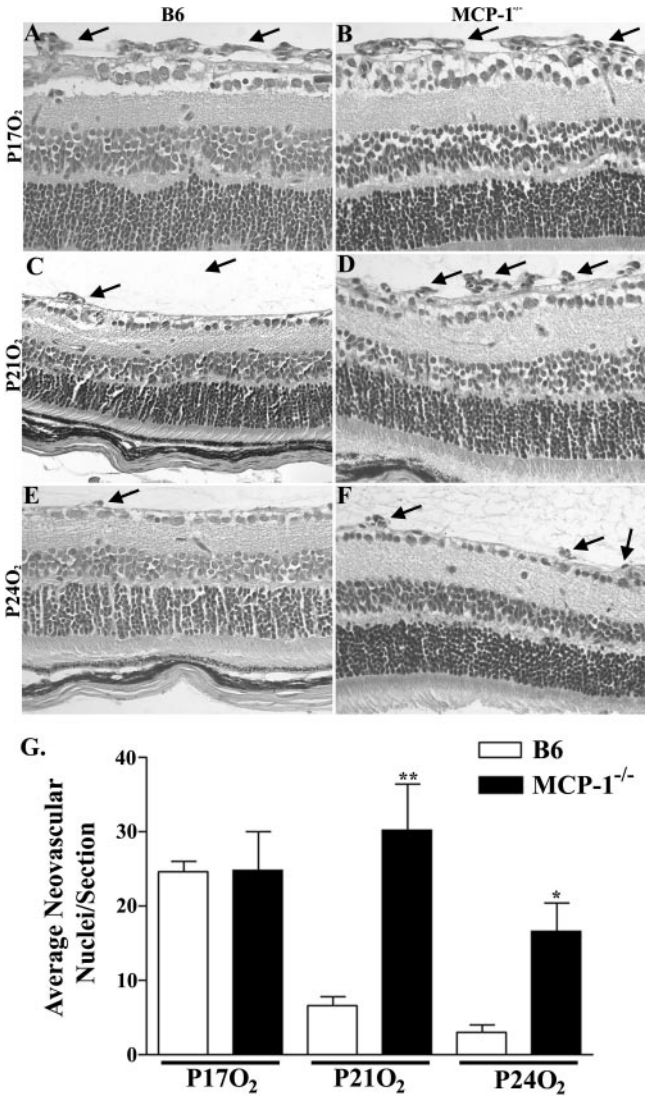

FIGURE 3. Delayed regression of NV in MCP-$1^{-/-}$ mice. Preretinal nuclei (*arrows*) in B6 (**A**, **C**, **E**) and MCP-$1^{-/-}$ (**B**, **D**, **F**) mice on $P17O_2$, $P21O_2$, and $P24O_2$ were counted after hyperoxia exposure. Quantification of preretinal nuclei revealed a significant difference between B6 and MCP-$1^{-/-}$ mice on $P21O_2$ (**$P < 0.004$) and $P24O_2$ (*$P < 0.02$) (**G**). Original magnification, ×400.

Downloaded from iovs.arvojournals.org on 04/13/2021

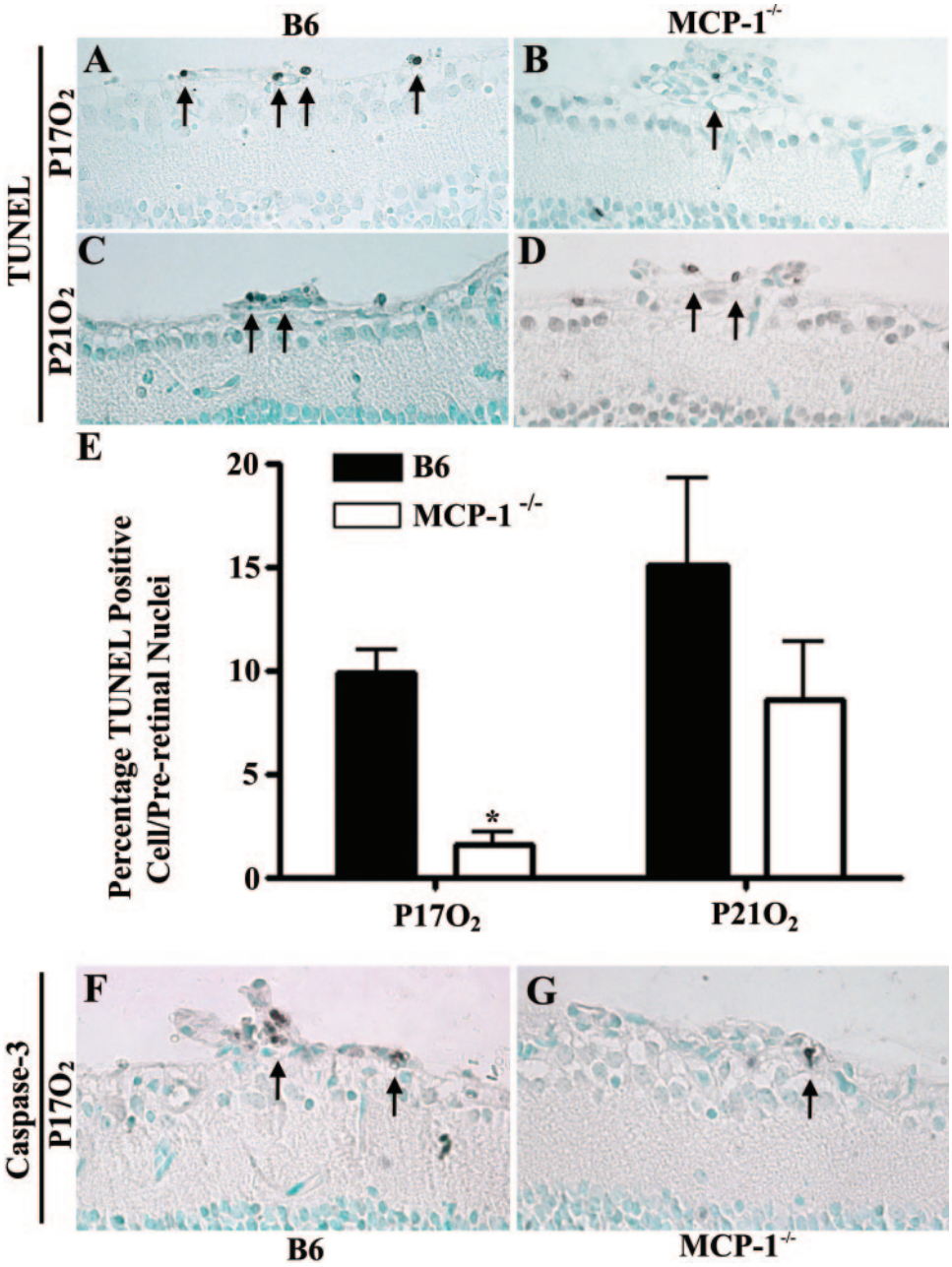

FIGURE 4. Decreased neovascular tuft apoptosis in MCP-$1^{-/-}$ mice. Representative TUNEL-stained sections from B6 (**A**, **C**) and MCP-$1^{-/-}$ (**B**, **D**) mice on $P17O_2$ and $P21O_2$. Apoptotic cells were observed within the neovascular tufts on $P17O_2$ in B6 mice (**A**, *arrows*) and, to a lesser extent, in MCP-$1^{-/-}$ (**B**, *arrows*) mice. On $P21O_2$, B6 mice (**C**, *arrows*) had numbers of apoptotic cells similar to those for MCP-$1^{-/-}$ mice (**D**, *arrows*). $TUNEL^+$ cells localized exclusively within the neovascular tufts were counted on $P17O_2$ and $P21O_2$ and were reported as a percentage of $TUNEL^+$ cells per neovascular nuclei (**E**). There was a significant difference between B6 and MCP-$1^{-/-}$ on $P17O_2$ (*$P < 0.0001$). Representative cleaved caspase-3–stained sections from B6 (**F**, *arrows*) and MCP-$1^{-/-}$ (**G**, *arrows*) mice on $P17O_2$. Original magnification, ×400.

Activated caspase-3 was also localized in $P17O_2$ sections. Qualitative assessment of the cleaved caspase-3 immunostaining demonstrated numerous positive cells localized to the neovascular tufts of B6 mice (Fig. 4F), whereas the neovascular tufts in the MCP-$1^{-/-}$ mice exhibited only an occasional caspase-3–positive cell (Fig. 4G).

DISCUSSION

Previous studies by our laboratory and others[22–24] have shown that macrophages/microglia colocalize with neovascular tufts in the mouse model of OIR and exhibit an associated increase in retinal MCP-1 expression. A recent study using in vivo immunostaining also confirms an intimate association between F4/80-labeled cells and retinal vessels in this model.[32] In vivo studies using transgenic models of MCP-1 overexpression confirm the important role this chemokine plays in the recruitment of monocytes and macrophages to sites of tissue expression.[33,34] Subsequently, MCP-$1^{-/-}$ mice were generated by targeted gene disruption to confirm the essential role of this chemokine in several models of inflammation and ischemia.[26–30] Similarly, in the present study, MCP-$1^{-/-}$ mice exhibited reduced recruitment of $F4/80^+$ cells, allowing us to examine the contribution of infiltrating macrophages to the pathogenesis of OIR. However, because microglia migrate to the retinal plexiform layers between P0 and P5 in response to macrophage colony-stimulating factor (MCSF), this $F4/80^+$ cell population was already present in the retina on P7, having migrated from its normal array in the plexiform layers to the anterior retina in response to oxygen-induced injury in B6 and MCP-$1^{-/-}$ mice.[21,35] Hence, the neovascular tufts in the MCP-$1^{-/-}$ mice showed a significant reduction in tuft-associated $F4/80^+$ cells but were not devoid of this cell population.

A balance between angiogenic and antiangiogenic factors determines whether vascular remodeling (regression) rather than vascular stabilization occurs after the initiation of retinal

Downloaded from iovs.arvojournals.org on 04/13/2021

NV.[36] VEGF and other angiogenic cytokines (antiapoptotic) have been well characterized for their contribution to NV in the mouse model of OIR.[37] In contrast, Fas/FasL, endostatin, and thrombospondin-1 are known to serve as negative regulators of angiogenesis through the induction of EC apoptosis in the OIR model.[5,38,39] Reduced vascular tuft apoptosis on P17 in the MCP-$1^{-/-}$ mice correlated with reduced numbers of vascular tuft F4/80^{+} cells, suggesting that macrophages/microglia may play a role in tuft regression through the induction of EC apoptosis. Similarly, in a model of choroidal neovascularization (CNV) induced by subretinal injection of basement membrane matrix (Matrigel; BD Biosciences, Franklin Lakes, NJ), MCP-$1^{-/-}$ mice develop more CNV in conjunction with reduced macrophages in the subretinal lesion.[40] In addition, after laser injury to the retina, FasL is downregulated in ocular macrophages of old mice, with an associated enhancement of CNV, compared with young mice.[41] A recent study using an experimental model of retinal detachment also confirmed the ability of activated macrophages/microglia to induce apoptosis in target cells in the eye through Fas/FasL, whereas a reduction in apoptosis was observed in MCP-$1^{-/-}$ mice.[42] We have also observed that TRAIL-deficient mice exhibit increased retinal NV on P17 and delayed regression of the vascular tufts on P21 in the OIR model (Hubert KE, et al. *IOVS* 2008;49:ARVO E-Abstract 3295). TRAIL expression was also colocalized with a subset of tuft-associated F4/80^{+} cells in control B6 mice, suggesting that macrophages/microglia may induce EC apoptosis and contribute to vascular tuft regression by TRAIL. In addition to the classic death receptor pathways, nitric oxide and hypochlorous acid are two macrophage products that have been characterized as mediators of EC apoptosis.[43,44] Ocular macrophages are also required for EC apoptosis during regression of the ocular capillaries in normal eye development, which has now been shown to be mediated by WNT7b.[16,45] Taken together, these studies support the concept that macrophages/microglia are capable of inducing endothelial apoptosis through a variety of proapoptotic pathways in the normal and diseased eye.

Despite endogenous proangiogenic properties of MCP-1, we did not observe a reduction in NV on P17 in the MCP-$1^{-/-}$ mice compared with B6 mice.[46–48] In addition, the unaltered NV observed on P17 in MCP-$1^{-/-}$ mice suggested that infiltrating macrophages are not a major contributor to NV in this model. These observations are consistent with Müller cell-derived VEGF playing the major role in stimulating angiogenesis in this model, as previously described.[49] However, with reduced numbers of infiltrating macrophages, the shift toward tuft regression that normally occurs in B6 mice between P17 and P21 is delayed in MCP-$1^{-/-}$ mice. Similarly, in a preliminary study in B6 mice, macrophages were systemically depleted with liposomal-clodronate, resulting in a reduction in neovascular tuft-associated F4/80^{+} cells with an associated twofold increase in neovascular nuclei on P21O_2, supporting the concept that infiltrating macrophages contribute to tuft regression (Davies MH, et al. *IOVS* 2006;47:ARVO E-Abstract 3223). In contrast to the MCP-$1^{-/-}$ mice, mice deficient in the intracellular apoptosis inhibitor Bcl-2 exhibit significantly less NV than B6 control mice in the OIR model.[50] In vivo studies using capillary tube assays revealed a requirement of only 22% apoptotic ECs for a significant decrease in microvascular density.[51] Hence, it appears that the B6 mice had a level of EC apoptosis that allowed for tuft regression between P17 and P21 in contrast to the delayed regression we observed in the MCP-$1^{-/-}$ mice, whereas Bcl-$2^{-/-}$ mice likely had a level of apoptosis that did not allow for a significant level of NV, despite the presence of VEGF. However, the vascular tufts eventually regressed in the MCP-$1^{-/-}$ mice, suggesting that additional apoptotic mechanisms lead to tuft regression after P21. We did observe an increase in the percentage of tuft cells undergoing apoptosis in the MCP-$1^{-/-}$ mice on P21. Growth factor withdrawal secondary to waning levels of retinal VEGF likely contributed to the eventual regression of the vascular tufts after P21 in the MCP-$1^{-/-}$ mice.[49] Retinal Fas was also up-regulated on P21 in the OIR model, whereas EC up-regulated this death receptor under irregular flow conditions (vascular tufts).[5,52] Thus, the tuft ECs in the nascent capillaries were vulnerable to autoregulatory FasL-induced cell death from neighboring ECs.[52] Finally, the resident microglia likely also contributed to eventual regression of the neovascular tufts.

Macrophages have been shown to exhibit distinct functions during injury and repair, with early-arriving macrophages promoting tissue injury and late-arriving macrophages promoting tissue recovery through the induction of apoptosis.[14,53] The concept of macrophages/microglia promoting vascular tuft regression through apoptosis does not exclude a proangiogenic function for these cells during an earlier phase in the OIR model. In fact, two recent studies have explored the contribution of microglia to the development of the retinal vasculature and the retinal response to oxygen-induced injury during the phase of hyperoxia exposure.[54,55] These studies suggest that microglia play a survival-promoting role for the nascent vessels in the immature retina. In models of laser-induced CNV, macrophages are localized to sites of tissue injury before the onset of NV, and systemic macrophage depletion results in reduced pathologic NV.[56,57] Hence, in an inflammatory model with an infiltration of macrophages and neutrophils before NV, the macrophages appear to play a significant role in promoting angiogenesis. However, in the OIR model, macrophages/microglia are localized to the neovascular tufts on P17 and P21, peaking well after the onset of NV.[22] We have also previously reported that neutrophil infiltration is not observed in the mouse model of OIR, supporting the notion that this model is not a proinflammatory model.[58] Alternatively, in a rat model of ischemia-induced NV, depletion of monocytes/macrophages leads to the suppression of retinal NV, supporting an angiogenic role for infiltrating macrophages in the context of this model and species.[59] Macrophages have also been linked to tumor angiogenesis, specifically when they are localized to regions of tumor hypoxia, where they release proangiogenic cytokines.[17] Even in the same tumor, macrophages can display distinct and alternative functions, depending on the local microenvironment.[60] Hence, macrophages/microglia have the potential to play many different roles in the processes of inflammation, angiogenesis, vascular regression, and neoplasia, depending on the temporal, spatial, and species biological context.

In summary, we demonstrate that the absence of MCP-1 expression in the mouse model of OIR results in reduced infiltration of macrophages, reduced vascular tuft apoptosis, and delayed regression of retinal NV. This suggests that the normal vascular regression observed in this model could potentially be mediated by the proapoptotic properties of macrophages/microglia. Further characterization of macrophage/microglia factors that induce retinal EC apoptosis may lead to new pharmacologic approaches in treating pathologic retinal NV, such as using intravitreal injection of soluble FasL or TRAIL.

References

1. Carmeliet P, Tessier-Lavigne M. Common mechanisms of nerve and blood vessel wiring. *Nature*. 2005;436(7048):193–200.
2. Das A, McGuire PG. Retinal and choroidal angiogenesis: pathophysiology and strategies for inhibition. *Prog Retin Eye Res*. 2003; 22(6):721–748.
3. Folkman J. Angiogenesis and apoptosis. *Semin Cancer Biol*. 2003; 13(2):159–167.

Downloaded from iovs.arvojournals.org on 04/13/2021

4. Kaplan HJ, Leibole MA, Tezel T, Ferguson TA. Fas ligand (CD95 ligand) controls angiogenesis beneath the retina. *Nat Med*. 1999; 5(3):292–297.
5. Davies MH, Eubanks JP, Powers MR. Increased retinal neovascularization in Fas ligand-deficient mice. *Invest Ophthalmol Vis Sci*. 2003;44(7):3202–3210.
6. Barreiro R, Schadlu R, Herndon J, Kaplan HJ, Ferguson TA. The role of Fas-FasL in the development and treatment of ischemic retinopathy. *Invest Ophthalmol Vis Sci*. 2003;44(3):1282–1286.
7. Volpert OV, Zaichuk T, Zhou W, et al. Inducer-stimulated Fas targets activated endothelium for destruction by anti-angiogenic thrombospondin-1 and pigment epithelium-derived factor. *Nat Med*. 2002;8(4):349–357.
8. Boyle JJ, Weissberg PL, Bennett MR. Human macrophage-induced vascular smooth muscle cell apoptosis requires NO enhancement of Fas/Fas-L interactions. *Arterioscler Thromb Vasc Biol*. 2002; 22(10):1624–1630.
9. Duffield JS, Erwig LP, Wei X, et al. Activated macrophages direct apoptosis and suppress mitosis of mesangial cells. *J Immunol*. 2000;164(4):2110–2119.
10. Koizumi K, Poulaki V, Doehmen S, et al. Contribution of TNF-alpha to leukocyte adhesion, vascular leakage, and apoptotic cell death in endotoxin-induced uveitis in vivo. *Invest Ophthalmol Vis Sci*. 2003;44(5):2184–2191.
11. Ashton AW, Ware GM, Kaul DK, Ware JA. Inhibition of tumor necrosis factor alpha-mediated NFκB activation and leukocyte adhesion, with enhanced endothelial apoptosis, by G protein-linked receptor (TP) ligands. *J Biol Chem*. 2003;278(14):11858–11866.
12. Halaas O, Vik R, Ashkenazi A, Espevik T. Lipopolysaccharide induces expression of APO2 ligand/TRAIL in human monocytes and macrophages. *Scand J Immunol*. 2000;51(3):244–250.
13. Li JH, Kirkiles-Smith NC, McNiff JM, Pober JS. TRAIL induces apoptosis and inflammatory gene expression in human endothelial cells. *J Immunol*. 2003;171(3):1526–1533.
14. Duffield JS, Forbes SJ, Constandinou CM, et al. Selective depletion of macrophages reveals distinct, opposing roles during liver injury and repair. *J Clin Invest*. 2005;115(1):56–65.
15. Lang R, Lustig M, Francois F, Sellinger M, Plesken H. Apoptosis during macrophage-dependent ocular tissue remodelling. *Development*. 1994;120(12):3395–3403.
16. Lobov IB, Rao S, Carroll TJ, et al. WNT7b mediates macrophage-induced programmed cell death in patterning of the vasculature. *Nature*. 2005;437(7057):417–421.
17. Crowther M, Brown NJ, Bishop ET, Lewis CE. Microenvironmental influence on macrophage regulation of angiogenesis in wounds and malignant tumors. *J Leukoc Biol*. 2001;70(4):478–490.
18. Barbera-Guillem E, Nyhus JK, Wolford CC, Friece CR, Sampsel JW. Vascular endothelial growth factor secretion by tumor-infiltrating macrophages essentially supports tumor angiogenesis, and IgG immune complexes potentiate the process. *Cancer Res*. 2002; 62(23):7042–7049.
19. Oh H, Takagi H, Takagi C, et al. The potential angiogenic role of macrophages in the formation of choroidal neovascular membranes. *Invest Ophthalmol Vis Sci*. 1999;40(9):1891–1898.
20. Grossniklaus HE, Ling JX, Wallace TM, et al. Macrophage and retinal pigment epithelium expression of angiogenic cytokines in choroidal neovascularization. *Mol Vis*. 2002;8:119–126.
21. Hume DA, Perry VH, Gordon S. Immunohistochemical localization of a macrophage-specific antigen in developing mouse retina: phagocytosis of dying neurons and differentiation of microglial cells to form a regular array in the plexiform layers. *J Cell Biol*. 1983;97(1):253–257.
22. Davies MH, Eubanks JP, Powers MR. Microglia and macrophages are increased in response to ischemia-induced retinopathy in the mouse retina. *Mol Vis*. 2006;12:467–477.
23. Yoshida S, Yoshida A, Ishibashi T, Elner SG, Elner VM. Role of MCP-1 and MIP-1α in retinal neovascularization during postischemic inflammation in a mouse model of retinal neovascularization. *J Leukoc Biol*. 2003;73(1):137–144.
24. Banin E, Dorrell MI, Aguilar E, et al. T2-TrpRS inhibits preretinal neovascularization and enhances physiological vascular regrowth in OIR as assessed by a new method of quantification. *Invest Ophthalmol Vis Sci*. 2006;47(5):2125–2134.
25. Smith LE, Wesolowski E, McLellan A, et al. Oxygen-induced retinopathy in the mouse. *Invest Ophthalmol Vis Sci*. 1994;35(1): 101–111.
26. Lu B, Rutledge BJ, Gu L, et al. Abnormalities in monocyte recruitment and cytokine expression in monocyte chemoattractant protein 1-deficient mice. *J Exp Med*. 1998;187(4):601–608.
27. Chae P, Im M, Gibson F, Jiang Y, Graves DT. Mice lacking monocyte chemoattractant protein 1 have enhanced susceptibility to an interstitial polymicrobial infection due to impaired monocyte recruitment. *Infect Immun*. 2002;70(6):3164–3169.
28. Tesch GH, Schwarting A, Kinoshita K, et al. Monocyte chemoattractant protein-1 promotes macrophage-mediated tubular injury, but not glomerular injury, in nephrotoxic serum nephritis. *J Clin Invest*. 1999;103(1):73–80.
29. Gu L, Okada Y, Clinton SK, et al. Absence of monocyte chemoattractant protein-1 reduces atherosclerosis in low density lipoprotein receptor-deficient mice. *Mol Cell*. 1998;2(2):275–281.
30. Hughes PM, Allegrini PR, Rudin M, et al. Monocyte chemoattractant protein-1 deficiency is protective in a murine stroke model. *J Cereb Blood Flow Metab*. 2002;22(3):308–317.
31. Connolly SE, Hores TA, Smith LE, D'Amore PA. Characterization of vascular development in the mouse retina. *Microvasc Res*. 1988; 36(3):275–290.
32. Shen J, Xie B, Dong A, et al. In vivo immunostaining demonstrates macrophages associate with growing and regressing vessels. *Invest Ophthalmol Vis Sci*. 2007;48(9):4335–4341.
33. Fuentes ME, Durham SK, Swerdel MR, et al. Controlled recruitment of monocytes and macrophages to specific organs through transgenic expression of monocyte chemoattractant protein-1. *J Immunol*. 1995;155(12):5769–5776.
34. Gu L, Rutledge B, Fiorillo J, et al. In vivo properties of monocyte chemoattractant protein-1. *J Leukoc Biol*. 1997;62(5):577–580.
35. Cecchini MG, Dominguez MG, Mocci S, et al. Role of colony stimulating factor-1 in the establishment and regulation of tissue macrophages during postnatal development of the mouse. *Development*. 1994;120(6):1357–1372.
36. Sakamaki K. Regulation of endothelial cell death and its role in angiogenesis and vascular regression. *Curr Neurovasc Res*. 2004; 1(4):305–315.
37. Saint-Geniez M, D'Amore PA. Development and pathology of the hyaloid, choroidal and retinal vasculature. *Int J Dev Biol*. 2004; 48(8–9):1045–1058.
38. Zhang M, Yang Y, Yan M, Zhang J. Downregulation of vascular endothelial growth factor and integrin β3 by endostatin in a mouse model of retinal neovascularization. *Exp Eye Res*. 2006;82(1): 74–80.
39. Wang S, Wu Z, Sorenson CM, Lawler J, Sheibani N. Thrombospondin-1–deficient mice exhibit increased vascular density during retinal vascular development and are less sensitive to hyperoxia-mediated vessel obliteration. *Dev Dyn*. 2003;228(4): 630–642.
40. Shen D, Wen R, Tuo J, Bojanowski CM, Chan CC. Exacerbation of retinal degeneration and choroidal neovascularization induced by subretinal injection of Matrigel in CCL2/MCP-1–deficient mice. *Ophthalmic Res*. 2006;38(2):71–73.
41. Kelly J, Khan AA, Yin J, Ferguson TA, Apte RS. Senescence regulates macrophage activation and angiogenic fate at sites of tissue injury in mice. *J Clin Invest*. 2007;117(11):3421–3426.
42. Nakazawa T, Hisatomi T, Nakazawa C, et al. Monocyte chemoattractant protein 1 mediates retinal detachment-induced photoreceptor apoptosis. *Proc Natl Acad Sci U S A*. 2007;104(7):2425–2430.
43. Kipari T, Cailhier JF, Ferenbach D, et al. Nitric oxide is an important mediator of renal tubular epithelial cell death in vitro and in murine experimental hydronephrosis. *Am J Pathol*. 2006;169(2): 388–399.
44. Sugiyama S, Kugiyama K, Aikawa M, et al. Hypochlorous acid, a macrophage product, induces endothelial apoptosis and tissue factor expression: involvement of myeloperoxidase-mediated oxidant in plaque erosion and thrombogenesis. *Arterioscler Thromb Vasc Biol*. 2004;24(7):1309–1314.
45. Diez-Roux G, Argilla M, Makarenkova H, Ko K, Lang RA. Macrophages kill capillary cells in G1 phase of the cell cycle during

Downloaded from iovs.arvojournals.org on 04/13/2021

programmed vascular regression. *Development*. 1999;126(10):2141–2147.

46. Hong KH, Ryu J, Han KH. Monocyte chemoattractant protein-1-induced angiogenesis is mediated by vascular endothelial growth factor-A. *Blood*. 2005;105(4):1405–1407.
47. Salcedo R, Ponce ML, Young HA, et al. Human endothelial cells express CCR2 and respond to MCP-1: direct role of MCP-1 in angiogenesis and tumor progression. *Blood*. 2000;96(1):34–40.
48. Stamatovic SM, Keep RF, Mostarica-Stojkovic M, Andjelkovic AV. CCL2 regulates angiogenesis via activation of Ets-1 transcription factor. *J Immunol*. 2006;177(4):2651–2661.
49. Pierce EA, Avery RL, Foley ED, Aiello LP, Smith LE. Vascular endothelial growth factor/vascular permeability factor expression in a mouse model of retinal neovascularization. *Proc Natl Acad Sci U S A*. 1995;92(3):905–909.
50. Wang S, Sorenson CM, Sheibani N. Attenuation of retinal vascular development and neovascularization during oxygen-induced ischemic retinopathy in Bcl-2−/− mice. *Dev Biol*. 2005;279(1):205–219.
51. Dong Z, Zeitlin BD, Song W, et al. Level of endothelial cell apoptosis required for a significant decrease in microvessel density. *Exp Cell Res*. 2007;313(16):3645–3657.
52. Sata M, Walsh K. Oxidized LDL activates fas-mediated endothelial cell apoptosis. *J Clin Invest*. 1998;102(9):1682–1689.
53. Friedman SL. Mac the knife? Macrophages—the double-edged sword of hepatic fibrosis. *J Clin Invest*. 2005;115(1):29–32.
54. Checchin D, Sennlaub F, Levavasseur E, Leduc M, Chemtob S. Potential role of microglia in retinal blood vessel formation. *Invest Ophthalmol Vis Sci*. 2006;47(8):3595–3602.
55. Ritter MR, Banin E, Moreno SK, et al. Myeloid progenitors differentiate into microglia and promote vascular repair in a model of ischemic retinopathy. *J Clin Invest*. 2006;116(12):3266–3276.
56. Tsutsumi C, Sonoda KH, Egashira K, et al. The critical role of ocular-infiltrating macrophages in the development of choroidal neovascularization. *J Leukoc Biol*. 2003;74(1):25–32.
57. Espinosa-Heidmann DG, Suner IJ, Hernandez EP, et al. Macrophage depletion diminishes lesion size and severity in experimental choroidal neovascularization. *Invest Ophthalmol Vis Sci*. 2003;44(8):3586–3592.
58. Powers MR, Davies MH, Eubanks JP. Increased expression of chemokine KC, an interleukin-8 homologue, in a model of oxygen-induced retinopathy. *Curr Eye Res*. 2005;30(4):299–307.
59. Ishida S, Usui T, Yamashiro K, et al. VEGF164-mediated inflammation is required for pathological, but not physiological, ischemia-induced retinal neovascularization. *J Exp Med*. 2003;198(3):483–489.
60. Lewis CE, Pollard JW. Distinct role of macrophages in different tumor microenvironments. *Cancer Res*. 2006;66(2):605–612.

Downloaded from iovs.arvojournals.org on 04/13/2021